Nonlinear dynamics induced in liquid crystals in the presence of the orbital and spin angular momentum of light

B. Piccirillo,* A. Vella,† A. Setaro,‡ and E. Santamato§
Dipartimento di Scienze Fisiche, via Cintia, 80126 Napoli, Italy
(Received 4 August 2005; revised manuscript received 16 December 2005; published 19 June 2006)

We studied the dynamical effects induced in a homeotropic nematic film when a normally incident circularly polarized light beam with an elliptical intensity profile is used. A three-dimensional dynamical model shows that, besides the spin, the orbital angular momentum of photons also plays a role in the reorientation process. Our measurements fairly reproduce the main dynamical features predicted by the model in the near threshold region. The model, however, does not work, as it is, at higher incident laser power where chaotic director rotation was reported [A. Vella, A. Setaro, B. Piccirillo, E. Santamato, Phys. Rev. E **67**, 051704 (2003)].

DOI: 10.1103/PhysRevE.73.062701 PACS number(s): 42.70.Df, 42.65.−k, 61.30.Gd

Liquid crystals (LCs) are unique optical materials because of their sensitivity to the angular momentum of light. The coupling of liquid crystals to the photon spin angular momentum (SAM) was clearly demonstrated by a series of experiments where homeotropically aligned nematic films were put into rotation by a circularly polarized laser beam at normal incidence [1–3]. The photon spin deposited in the medium may lead to complex light-induced dynamics exhibiting a nontrivial sequence of bifurcations [4–6]. Recently, it was suggested that liquid crystals could be sensitive to the photon orbital angular momentum (OAM) too [7,8] and a series of works appeared on this subject [9–12], inspired by the seminal paper by Allen *et al.* [13]. In all these works, the transfer of the OAM of light to the nematic liquid crystal (NLC) film was achieved by means of a normally incident laser beam with elliptical rather than circular intensity profile. The transfer of photon OAM requires light beams having a finite noncylindrically symmetric cross section. Light beams cylindrically symmetric around their propagation axis, in fact, cannot exchange OAM with transparent media endowed with a smooth refractive index distribution, such as liquid crystals. With the exception of Ref. [9], where a circularly polarized beam was used, in all the above-cited works, concerning the OAM transfer to liquid crystals, linearly polarized light was used. Using circular rather than linear polarization, however, is desirable since the effects produced by the photon OAM could be highlighted by comparison to the dynamical features observed in the case of pure photon SAM transfer. For example, many experiments proved that, in the case of a circularly shaped and circularly polarized incident beam, no stationary states may exist above the optical Fréedericksz transition (OFT) threshold, whatever the light intensity is, as one can find in the literature. This is because as soon as the sample comes to be reoriented, a finite amount of light SAM is transferred into the medium, producing an unbalanced overall torque along the beam direction. If the beam cross section is elliptical, instead, the light OAM provides a new source of optical torque that, just above the reorientation threshold, can balance the SAM transfer, yielding stationary distorted states. Thus, the existence of stationary-state branches is a distinctive feature of the occurrence of photon OAM transfer, when a circularly polarized incident beam is used. Stationary-state branches may occur also when a circularly shaped and elliptically polarized beam is used [14–16]. In this case, in fact, elastic configurations of the LC can be realized, where the SAM transfer is zero (the overall effect is just rotating the polarization ellipse axis) and no azimuthal optical torque is produced. This internal balancing mechanism of photon SAM transfer is forbidden in the case of circular polarization. One of the main results for the present work is the experimental proof of the existence of such a stationary-state branch, which is also confirmed by a preliminary three-dimensional (3D) model we worked out adapting the model reported in Ref. [12] to a circularly polarized incident beam. Although our observations provide a somewhat indirect proof of OAM transfer in LC, we think this could be valuable as an accurate direct method for measuring the OAM deposited by photons in the sample.

The experimental geometry considered in this work is as follows: a circularly polarized Gaussian-shaped laser beam with different waists ($1/e^2$ intensity) w_x and w_y along fixed x and y directions impinges at normal incidence onto a homeotropically aligned NLC film of thickness L. In our experiments, we used a frequency-doubled $Nd:YVO_4$ laser beam at $\lambda=532$ nm. The polarization of the beam was made circular by means of a quarter wave plate, and the beam shape at the sample position was made elliptical by means of two cylindrical lenses to have $I(x,y)=I_0\exp[-2(x^2/w_x^2+y^2/w_y^2)]$, where $w_x=100$ μm and where $w_y=10$ μm. The sample was a 50 μm thick film of E7 NLC from Merck confined by parallel glass walls coated with DMOAP for homeotropic strong anchoring. The laser-induced dynamics of the director $\boldsymbol{n}$ was deduced from the polarization of the outer rings in the far-field diffraction pattern and, simultaneously, from the diameter of the outmost ring as a function of time. Further details about the apparatus and the data analysis for reconstructing the motion of $\boldsymbol{n}$ have been reported elsewhere [17]. Only to study the stationary states just above the OFT threshold (circles in Fig. 1), where the previous technique could not be applied, we measured the polarization change of a

*Electronic address: bruno.piccirillo@na.infn.it
†Electronic address: angela.vella@na.infn.it
‡Electronic address: antonio.setaro@na.infn.it
§Electronic address: enrico.santamato@na.infn.it

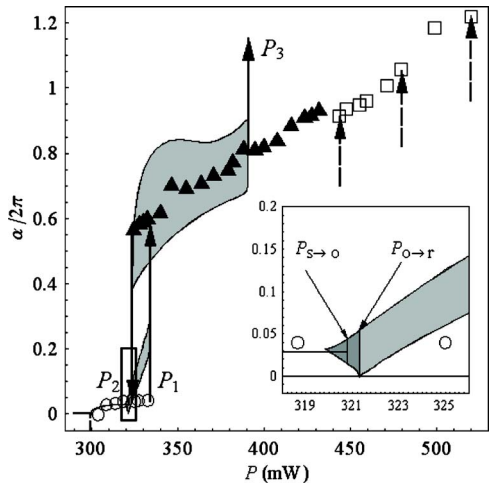

FIG. 1. (Color online) The optical phase difference α in unit of 2π as function of the incident power P. ○ stationary states; ▲ rotations; □ intermittent states. The shadowed regions represent the oscillation amplitude of α and the experimental points mark the oscillation center. The broken line arrows mark the intermittent states studied in Ref. [1].

circularly polarized He-Ne probe beam copropagating with the pump.

Our model was based on the Ritz' method applied to the total (elastic+optical) free energy $\mathcal{F}=\int_V FdV$ and dissipation function $\mathcal{R}=\int_V RdV$ of the sample, generalizing the scheme adopted in Ref. [12]. All three space coordinates and time have been retained and the elastic anisotropy of the material was also taken into account. The parameters $p_i(t)$ $(i=1,\ldots,6)$ of our model are the maximum tilt angle $\theta_0(t)$, the rotation angle $\phi_0(t)$, the torsion angle $\phi_1(t)$, and the three quantities $\theta_1(t)$, $\theta_2(t)$, and $\gamma(t)$, characterizing the two semiaxes and the orientation angle of the θ transverse profile, respectively (for definitions, see Ref. [12]). A set of ODEs for the dimensionless parameters $p_i(t)$ was obtained by evaluating the functionals $\mathcal{F}$ and $\mathcal{R}$ and solving with respect to the time derivatives $\dot{p}_i(t)=dp_i/dt$ the torque equations $\mathcal{T}_i \equiv \frac{\partial \mathcal{F}}{\partial p_i}=\frac{\partial \mathcal{R}}{\partial \dot{p}_i}$ $(i=1,\ldots,6)$. The approximations exploited in the model were the same as in Ref. [12], namely, small LC elastic distortion, adiabatic propagation of light along the beam axis only, and uniform polarization in the beam transverse plane. The ODEs of our model have the general form $\dot{p}_i=A_{ij}(p)\mathcal{T}_j$, where $A_{ij}(p)$ is a 6×6 matrix. The elastic contributions to the torques $\mathcal{T}_i$ are $\mathcal{T}_i^e=\partial\mathcal{F}^e/\partial p_i$, where the elastic free energy $\mathcal{F}^e$ has the form

$$\mathcal{F}^e = F_0\{T_0 + T_1(\theta_2^{-2}+\theta_1^{-2}) + T_2(\theta_2^{-2}-\theta_1^{-2})\cos[2(\gamma-\phi_0)]\}, \tag{1}$$

where $F_0=\frac{\pi k_{33} L\theta_1\theta_2}{8}$ (k_{33} is the LC elastic constant for bend distortion) and T_k $(k=0,1,2)$ are polynomials in the small quantities θ_0 and ϕ_1. From Eq. (1), we see that the elastic torques $\mathcal{T}_{\phi_0}^e$ and $\mathcal{T}_\gamma^e$ are opposite and given by $\mathcal{T}_{\phi_0}^e=-\mathcal{T}_\gamma^e$ $=2F_0T_2(\theta_2^{-2}-\theta_1^{-1})\sin[2(\gamma-\phi_0)]$. These torques vanish when $\gamma=\phi_0$, i.e., when the average azimuthal angle of the director $\boldsymbol{n}$ is aligned along the major axis of the transverse θ distribution. The elastic torques $\mathcal{T}_{\phi_0}^e$ and $\mathcal{T}_\gamma^e$ are internal to the system and originate from the lack of symmetry of $\mathcal{F}^e$ under rotation of $\boldsymbol{n}$ in the transverse plane. Within the same approximation, the optical contributions $\mathcal{T}_{\phi_0}^o$ and $\mathcal{T}_\gamma^o$ to the torques acting on ϕ_0 and γ are given by

$$\mathcal{T}_{\phi_0}^o = \frac{\sigma P}{\omega}\left\{Z_1(1-\cos\alpha) - \frac{\alpha^2 G(\alpha)}{6\beta}[3\delta Z_1 + 2(2-6\delta)Z_2]\right\} \tag{2a}$$

$$\mathcal{T}_\gamma^o = -\frac{P}{\omega}(\theta_1^{-2}-\theta_2^{-2})(w_x^2-w_y^2) \times\left\{\frac{Z_1^3\alpha}{16} - \frac{\alpha^2}{128\beta}[3\delta Z_1^3 - 4(3\delta-1)Z_2^3]\right\}\sin 2\gamma, \tag{2b}$$

where $\sigma=\pm 1$ depending on the polarization helicity, P is the incident power, ω is the optical frequency, $\delta=1-n_o^2/n_e^2$ (n_e and n_o being the material extraordinary and ordinary refractive indices, respectively), $\alpha=\beta\theta_0^2$, with $\beta=\pi n_0\delta L/2\lambda$, is the small distortion expression for the phase difference accumulated by the extraordinary and ordinary waves in traversing the sample, and finally, $G(\alpha)=\int_0^1 du\,\sin^4(\pi u)\sin[\alpha(u-\sin\pi u/2\pi)]$. The quantities Z_1 and Z_2 in Eqs. (2) come from the average over the nonuniform transverse profiles of the light-induced refractive index and of the light intensity, viz. $Z_1=\theta_0^{-2}I_0^{-1}\int\theta^2 I dxdy$, $Z_2=\theta_0^{-4}I_0^{-1}\int\theta^4 I dxdy$. The right-hand side of Eq. (2a) may be identified as the expression for the overall photon SAM $(P/\omega)\Delta S_z$ and the right-hand side of Eq. (2b) as the expression for the overall photon OAM $(P/\omega)\Delta L_z$ transferred to the sample in our approximation (ΔS_z and ΔL_z refer to a single photon). Equations [2] clearly show that the photon spin acts on the azimuthal angle ϕ_0 of $\boldsymbol{n}$, whereas the photon OAM acts on the angle γ of the θ distribution, i.e., on the transverse gradients of **n**, thus confirming what was already obtained from more general principles [18]. According to Eq. (2b), ΔL_z is proportional to $\sin 2\gamma$ and vanishes for a circularly shaped $(w_x=w_y)$ laser beam. At stationary state, when the torques acting on ϕ_0 and γ are added together, the internal torques $\mathcal{T}_{\phi_0}^e$ and $\mathcal{T}_\gamma^e$ cancel out, and the equation for the total angular momentum balance reduces to $\Delta L_z+\Delta S_z=0$, as expected. The ODEs of our model were numerically solved for values of the material constants of E7 at room temperature as reported in Ref. [12].

The near-threshold results of our model are compared to our experimental findings in Fig. 1, where the phase difference α is plotted as a function of the incident laser power P. Circles correspond to the near threshold stationary states observed in the experiment. The transition from the undistorted state to this stationary-state branch at the OFT power threshold P_{th} is second order. As said above, this experimental result and the agreement with our model (full line, in Fig. 1) are the proof that some amount of photon OAM is transferred so to balance the SAM deposited in the sample. It is worth noting that our model allows one to explicitly calculate the OAM and SAM transfer ΔL_z and ΔS_z. Under our experimental conditions, the same model predicts that ΔS_z and ΔL_z are both nonzero and balance exactly at the station-

ary states reported in Fig. 1. When the power P is further increased, at critical power $P_1=334\pm1$ mW, a first-order transition to a rotating regime is observed (the higher shadowed region in Fig. 1), also in agreement with our model. The hysteresis loop shown in Fig. 1 is also fairly well reproduced. When the incident power is lowered to the value $P_2=324\pm1$ mW, in fact, the loop is closed and the system jumps back to the lower branch. If, instead, the power is increased, rotating states are observed (triangles in Fig. 1) until, at very high incident power, chaotic rotating states (squares in Fig. 1) are found as reported elsewhere [9]. Since the transition at P_1 can be located much better than all the other transitions, we scaled the OFT threshold power foreseen by our model to make the theoretical and experimental values of P_1 coincide. Just setting this single parameter, the observed OFT threshold power (300 ± 1 mW) was found very close to the theoretical prediction (299.6 mW, corresponding to a threshold intensity of 3.3 kW/cm^2 on the beam axis). In the loop region, however, we observed some discrepancies between theory and experiment. In our model, in fact, a first transition took place to an oscillating regime at $P_{s\to o}=320.8$ mW (see inset in Fig. 1) and, at slightly higher power $P_{o\to r}=321.3$ mW, a second transition occurred to a rotating regime via a gluing bifurcation similar to the one observed in the case of elliptical polarization of the incident beam [14]. In the experiment, we were not able to locate any bifurcations from stationary to oscillating ($s\to o$) and then rotating states ($o\to r$) along the lowest distorted branch. Very likely, because of the sensitivity limitations of our measurement technique, we were led to regard all the states between P_{th} and P_1 as stationary states (○ in Fig. 1), but the existence of such bifurcations cannot be excluded. Moreover, if the power is increased over $P_3=386.3$ mW, the model shows a jump to a highly distorted stationary state, not observed on experimental grounds. In the experiment, in fact, the rotating branch was observed to continue until the onset of the intermittent chaotic rotations (□ in Fig. 1) reported in Ref. [9], as mentioned above. The experimental oscillation amplitudes were not reported in Fig. 1), but they were found about 20% larger than predicted by theory. In Fig. 2, the period of the director azimuthal dynamics is reported as a function of the incident power. The presence of relatively large error bars in the figure is because the rotation period was fluctuating in time. At present, we cannot say if the period fluctuations are due to light-induced dynamic effects or to the presence of external noise. The dashed and solid lines labeled a,b,c were calculated from our model and correspond to the oscillating, the lower rotating, and the higher rotating regimes, respectively. The period divergence shown in Fig. 2 corresponds to the gluing bifurcation at $P=P_{o\to r}$. As said above, we observed the second rotating regime only, where, nevertheless, the agreement with theory turned to be fairly satisfactory, as shown in Fig. 2; although, some features predicted by the model remained undetected by our apparatus. The multiple stationary branches shown in Fig. 3(a) are an example. Moreover, in the lowest stationary-state branch just above the OFT threshold, a large out-of-plane reorientation is expected, as shown in Fig. 3(b). The angle ϕ_0 may reach values as large as 45°, after which the system jumps to the rotating state. At the same time, the stationary-state values of

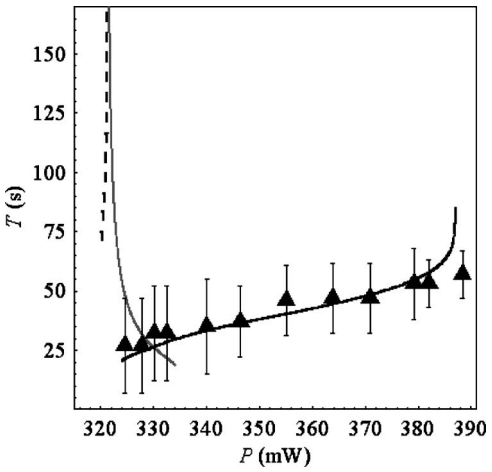

FIG. 2. The period of the director azimuthal dynamics as a function of the incident power P. The points with error bars refer to experiment and the lines to theory: (a) dashed line; oscillating branch; (b) continuous gray line, lower rotating branch; (c) continuous black line, higher rotating branch. Our data refer only to the last branch.

ϕ_1 and γ remain quite small (Figs. 3(c) and 3(d)). As a matter of fact, our apparatus was not designed to measure the transverse θ profile and, hence, the angle γ. Besides, evaluating ϕ_0 along the near threshold phase-locked stationary branch turned out to be problematic as well. In fact, when the molecular director $\boldsymbol{n}$ is nearly aligned along the axis of the probe beam, the phase change is small and the measurement of the orientation of the optical axis is affected by a large noise. At present, a more efficient experimental apparatus is under study to perform an accurate measurement of ϕ_0, on one hand, and to obtain information about the shape of the θ distribution, on the other hand. The model itself should be considered as preliminary and could be improved in many respects. First of all, the coupling between the ordinary and the extraordinary waves due to the torsion ϕ_1 [19], neglected

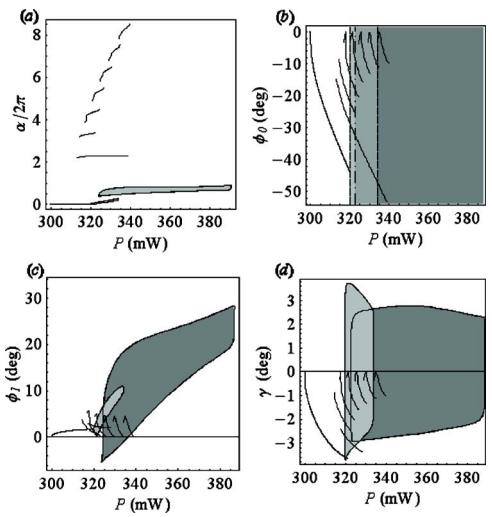

FIG. 3. (Color online) Dynamical features predicted by the theoretical model. The shadowed region refer to the variation amplitude of the dynamical variables in the time-varying regime.

in the present work because not relevant to the OAM issue, could be taken into account at least in the first perturbative approximation as already done in Ref. [12]. Moreover, our model was unable to predict the on-off intermittent rotational regime placed along the continuation of the higher rotating branch reported in Ref. [9], although it takes into account nonlocal effects due to the finite beam size and some experiments showed the appearance of chaotic regimes when a circularly polarized beam is used having a finite circular cross section [6]. Maybe the chaotic fatures could be recovered by introducing higher-order spatial modes in the expansion of θ and ϕ as made, for example, in Ref. [5].

In conclusion, we presented model and experiment to describe the simultaneous transfer of photon spin and orbital angular momenta to an NLC film. Although preliminary, our model grasps the essential physics in the near-threshold region and, in particular, the existence of stationary distorted states where the light spin and orbital angular momentum deposited in the sample balance each other. Oscillating as well as rotating regimes are foreseen by our model, but only the latter were observed in the experiment. The on-off intermittent rotation reported in Ref. [9] was not reproduced by the model, although these regimes lay along the continuation of the calculated rotation branch in Fig. 1. Significative improvements of both model and experiment are in progress.

We acknowledge financial support by the Dipartimento di Scienze Fisiche e Regione Campania L. 5.

[1] E. Santamato, B. Daino, M. Romagnoli, M. Settembre, and Y. R. Shen, Phys. Rev. Lett. **57**, 2423 (1986).
[2] E. Santamato, M. Romagnoli, M. Settembre, B. Daino, and Y. R. Shen, Phys. Rev. Lett. **61**, 113 (1988).
[3] T. V. Galstyan and V. Drnoyan, Phys. Rev. Lett. **78**, 2760 (1997).
[4] E. Brasselet, B. Doyon, T. V. Galstian, and L. J. Dubé, Phys. Rev. E **67**, 031706 (2003).
[5] E. Brasselet, T. V. Galstyan, L. J. Dubé, D. O. Krimer, and L. Kramer, J. Opt. Soc. Am. B **22**, 1671 (2005).
[6] E. Brasselet, B. Doyon, T. V. Galstian, and L. J. Dubé, Phys. Rev. E **69**, 021701 (2004).
[7] L. Marrucci, B. Piccirillo, and E. Santamato, J. Opt. Soc. Am. A **2**, 294 (2000).
[8] B. Piccirillo, C. Toscano, F. Vetrano, and E. Santamato, Phys. Rev. Lett. **86**, 2285 (2001).
[9] A. Vella, A. Setaro, B. Piccirillo, and E. Santamato, Phys. Rev. E **67**, 051704 (2003).
[10] B. Piccirillo, A. Vella, and E. Santamato, J. Opt. Soc. Am. B **4**, S20 (2002).
[11] B. Piccirillo, C. Toscano, and E. Santamato, Mol. Cryst. Liq. Cryst. Sci. Technol., Sect. A **372**, 383 (2002).
[12] B. Piccirillo, A. Vella, and E. Santamato, Phys. Rev. E **69**, 021702 (2004).
[13] L. Allen, M. W. Beijersbergen, R. J. C. Spreeuw, and J. P. Woerdman, Phys. Rev. A **45**, 8185 (1992).
[14] D. O. Krimer, L. Kramer, E. Brasselet, T. V. Galstian, and L. J. Dubé, J. Opt. Soc. Am. B **22**, 1681 (2005).
[15] E. Santamato, G. Abbate, P. Maddalena, L. Marrucci, and Y. R. Shen, Phys. Rev. Lett. **64**, 1377 (1990).
[16] A. Vella, B. Piccirillo, and E. Santamato, Phys. Rev. E **65**, 031706 (2002).
[17] E. Santamato, G. Abbate, P. Maddalena, L. Marrucci, D. Paparo, and B. Piccirillo, Mol. Cryst. Liq. Cryst. Sci. Technol., Sect. A **328**, 479 (1999).
[18] B. Piccirillo and E. Santamato, Phys. Rev. E **69**, 056613 (2004).
[19] V. V. Zheleznyakov, V. V. Kocharovskiĭ, and V. V. Kocharovskiĭ, Sov. Phys. JETP **52**, 877 (1980), [Zh. Eksp. Teor. Fiz. **79**, 10735–1758 (1980)].